Dalton Transactions

Accepted Manuscript

ROYAL SOCIETY OF CHEMISTRY

www.rsc.org/dalton

Graphical Absrtact

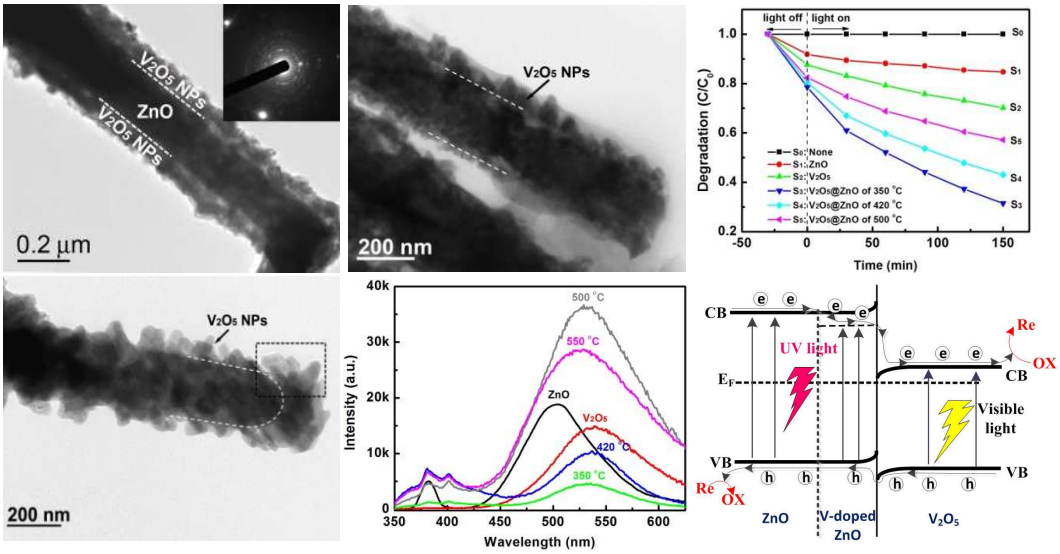

Different V_2O_5/ZnO heteronanorods were synthesized at different oxidization temperatures. Novel PL properties, including new PL peaks, the tuned PL intensity, and enhanced visible emission, were observed. Enhanced photocatalytic activities were obtained and the temperature influence was discussed. Novel PL properties and enhanced photocatalytic activities were attributed to the collective effect of V-doped ZnO layer at interface, decreased defect concentration, and improved particle crystallinity.

Dalton Transactions

RSCPublishing

PAPER

Novel Photoluminescence Properties and Enhanced Photocatalytic Activities for V_2O_5-Loaded ZnO Nanorods

Cite this: DOI: 10.1039/x0xx00000x

Received ooth January 2012,
Accepted ooth January 2012

DOI: 10.1039/x0xx00000x

www.rsc.org/

Haihong Yin,[ab] Ke Yu,[b*] Jingjing Hu,[a] Changqing Song,[a,b] Bangjun Guo,[b] Zhiliang Wang,[a] and Ziqiang Zhu[b]

Three different kinds of V_2O_5/ZnO heteronanorods were synthesized through a CVD process and oxidized in air at temperatures of 350, 420 and 500 °C. These 1D heteronanorods are formed by ZnO nanorods (NRs) coated with V_2O_5 nanoparticles (NPs). With the rise of oxidization temperature, the coated V_2O_5 NPs are found growing and their crystallinity gradually improved. Photoluminescence (PL) spectra for these V_2O_5/ZnO samples exhibited some novel characteristics, such as the appearance of new emission peaks, the variation in PL intensity, and the tremendously enhanced visible emission for the sample of 500 °C. Photocatalysis investigation for all V_2O_5/ZnO samples showed enhanced photocatalytic activities compared to their single-component counterparts. Furthermore, their photocatalytic activities were also influenced by the oxidization temperature. The sample of 350 °C showed the highest photocatalytic activity, and gradually decreased photocatalytic activities were observed for other two samples. The novel PL properties and enhanced photocatalytic activities were attributed to the coupling between ZnO NRs and V_2O_5 NPs, and can be interpreted by the collective effect of the V-doped ZnO layer near the interface, the decreased defect concentration in V_2O_5 NPs, and the improved particle crystallinity.

Introduction

Hybrid materials draw a lot of attention and effort for providing clues to develop new materials with improved performance or new useful properties.[1] Among them, combining different semiconductors at the nanoscale into a hybrid nanostructure has been an important research direction in the nanostructure synthesis. The band offset at the interface and the synergistic interactions between each component could strongly affect the final properties. As compared to their single-component counterparts, the properties of these heteronanostructures could be tuned both through composition and subtle structure control, often exhibiting improved properties in optoelectronics,[2] photovoltaic,[3] catalysis,[4] and bioengineering.[5]

ZnO nanostructure is an important semiconductor with a direct bandgap of 3.34 eV, and the primary motivator of ZnO research is its great potential for a variety of practical applications, such as in LEDs,[6] solar cells,[7] nanogenerators,[8] transistors,[9] sensors,[10] catalysts,[11] etc. In these applications, coupling ZnO with other compounds and forming heteronanostructures is a promising strategy to improve their physicochemical properties. For example, visible-light-driven photocatalytic properties have been observed in ZnO/$ZnFe_2O_4$ core/shell nanocable arrays.[12] Enhanced field emission performance with a large emission current has been demonstrated in MgO-loaded ZnO nanotetrapods.[13] In the light-emitting devices, ZnO nanostructures often exhibited two different emission bands including the ultraviolet emission (~380 nm) and the green emission (450~600 nm). How to control and tune the two emission bands is crucial for the actual application of ZnO light-emitting devices. In many literatures, a variety of strategies, such as doping,[14, 15] thermal annealing,[16-18] plasma treatment, [19, 20] and constructing heteronanostructures,[21, 22] have been developed. Among them, constructing ZnO heteronanostructures has been proved to be a feasible technique to improve ZnO luminescence properties.[23] However, the luminescence properties of ZnO-based heteronanostructures are strongly dependent on the actual synthesis environment and closely correlated to factors including the crystallinity, the coupling material properties, and the defect concentration.[17] For example, Jin et al. reported enhanced near-band edge (NBE) emission in ZnO-core/SnO_2-shell nanorods (NRs);[23] however, the opposite suppressed NBE emission was also reported by Kuang et al. in ZnO-core/SnO_2-shell nanostructures.[24] Obviously, the synthesis environment and the microstructure played a crucial role in the luminescence properties of ZnO-

based heteronanostructures. Thus, selecting an appropriate coupling material and studying the influence of synthesis environment are essential for the adjustment of the final luminescence performance.

V_2O_5, a semiconductor with a bandgap of 2.3 eV, is the most stable form of vanadium oxides. Previous reports have revealed that V_2O_5 showed visible photoluminescence (PL) and the emission intensity strongly depends on its microstructure.[25-27] In addition, enhanced visible luminescence was also observed in V_2O_5/ZnO bilayer;[28] however, the opposite enhanced NBE emission was observed in V_2O_5-coated ZnO NRs.[29] Thus, the microstructure and the synthesis parameters of 1D V_2O_5/ZnO heteronanostructures should play a crucial role, and their influence on the final optical properties should be detailedly investigated. Besides photoluminescence, the photocatalysis property of ZnO nanostructure has also been actively investigated owing to its high electron mobility, abundant morphologies, easy synthesis, and low cost.[4, 30] However, its large bandgap (~3.3 eV) only allows it absorbing UV light for the charge carrier generation, and the high recombination (~90%) hinders photogenerated electron−hole pairs migrating from the inner to the surface, leading to a low photodegradation efficiency under the solar irradiation. Up to now, several methods, such as doping,[31, 32] structure improvement,[33, 34] and surface modification,[35-37] have been proposed to prevent the recombination of photogenerated carrier pairs and extend the light-absorption range. In 1D V_2O_5/ZnO heteronanostructures, the combination of ZnO with V_2O_5 can enlarge the light absorption from UV to the visible region; meanwhile, the separation of photogenerated carriers is promoted at the interface due to the band offset, thus the enhanced photocatalytic activity should be expected. In this paper, V_2O_5/ZnO heteronanorods were prepared by coating V_2O_5 nanoparticles (NPs) on ZnO NRs through a CVD route followed by a thermal oxidization. By changing the oxidation temperature in the synthesis process, the crystallinity and size of the coated V_2O_5 NPs can be adjusted, and we focus on the effect of the particle size and their crystallinity on the final PL and photocatalytic properties.

Experimental Section

Synthesis of V_2O_5/ZnO heteronanorods The synthesis strategy for V_2O_5/ZnO heteronanorods is to synthesize ZnO NRs and then coated with V_2O_5 NPs. Briefly, a cleaned silicon (100) substrate was placed ~10 cm downstream of a quartz tube in a horizontal tubular furnace. Mixed ZnO power (purity 99.99%) and graphite powder (purity 99.9%) were loaded in a quartz boat and placed at the center of the furnace. Then, the central temperature was increased to 870 °C at a rate of 10 °C min^{-1} and held 60 min under a constant N_2 (purity 99.9%) flow of 400 sccm. After the furnace was cooled to room temperature, a light white ZnO layer was found being deposited on the substrate. Subsequently, V_2O_5 NPs were coated on the ZnO NRs using a CVD method. The silicon substrate covered with ZnO was located at the tube center of a CVD system. Vanadyl acetylacetonate ($VO(acac)_2$) was taken as vanadium precursors and placed in a special evaporating chamber, where temperature was controlled at 200 °C. Before heating, the CVD system was pumped to expel oxygen in the tube, and pure nitrogen gas was introduced to reach the pressure of atmosphere. Then, the reaction chamber was heated to 500 °C. A nitrogen flow (purity 99.9%) at a constant rate of 90 sccm was used to carry the precursor vapor to the reaction chamber. The reaction lasted for 30 min, and then the system was cooled down to room temperature under a N_2 flow, and the color of the product changed from light white to dark gray. After oxidizing them in air for 120 min, the color of the products changed from dark-gray to yellow, and V_2O_5/ZnO heteronanorods were finally obtained. When controlling the oxidization temperature at 350, 420, 500 and 550 °C, respectively, four different samples of V_2O_5/ZnO heteronanorods were obtained.

Characterization The morphologies and size of the product were characterized by field-emission scanning electron microscopy (FESEM, Hitachi-S-4800) and transmission electron microscopy (JEOL, JEM-2100). The crystal structure was characterized by X-ray diffraction (XRD, Bruker D8 Advance diffractometer using monochromatized Cu Kα radiation (λ = 1.5418Å). UV-visible spectra were recorded with a UNICO-2802 ultraviolet-visible spectrophotometer. PL spectra were measured on a fluorescence spectrometer (Edinburgh FLS920) by using a He–Cd laser (325 nm) as the excitation source. All measurements for the as-prepared samples are carried out at room temperature.

Photocatalysis Measurement The photocatalytic activities of pure ZnO, V_2O_5 and three V_2O_5/ZnO samples were evaluated by the degradation of MB at room temperature under ultraviolet-visible (UV-vis) light. The maximum optical absorption of MB at 664 nm was used to monitor the concentration. The as-fabricated photocatalysts (0.03 g) were added to a cylindrical container containing 100 mL MB aqueous solution (10 mg L^{-1}). Before irradiation, the solution was stirred in the dark for 30 min to ensure establishment of the equilibrium between adsorption and desorption. To minimize the heat effect, the photo reactor was fixed in a glass jacket and cooled by flowing water. The solution was irradiated with a tungsten halogen lamp ($\lambda \geq 340$ nm) to trigger the photocatalytic reaction. After recovering the photocatalyst by centrifugation, the MB concentration was analyzed by a UV-vis spectrophotometer (UNICO 2802) every 30 minutes during the total irradiation time of 150 minutes. The photocatalytic measurements for different photocatalysts (ZnO NRs, V_2O_5 NPs and different V_2O_5/ZnO samples) were performed in independent experiments.

Results and discussion

In the synthesis of V_2O_5/ZnO heteronanorods, $VO(acac)_2$ was decomposed under high temperature, an intermediate of V_2O_5 was coated on ZnO NRs through a CVD process, and a V_2O_5 encapsulation was finally formed on ZnO surface after a thermal oxidization process. To investigate the effect of the

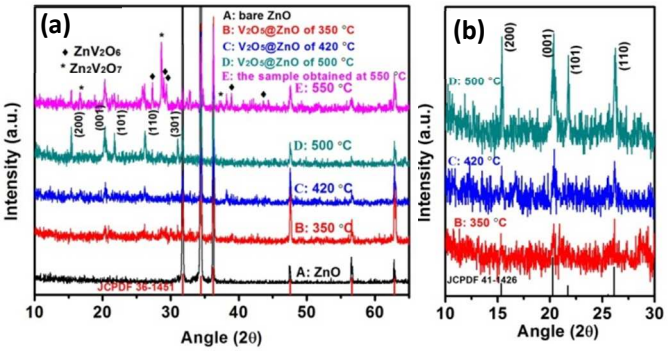

Fig. 1. (a) XRD patterns of bare ZnO NRs (A) and V_2O_5/ZnO heteronanorods obtained at different oxidization temperatures of 350 (B), 420 (C), 500 (D) and 550 °C (E), respectively. It is noted that some impurities of ZnV_2O_7 and ZnV_2O_6 appeared in the product of 550 °C. (b) The expanded view of XRD patterns for V_2O_5/ZnO heteronanorods obtained at 350 (B), 420 (C), 500 °C (D), respectively.

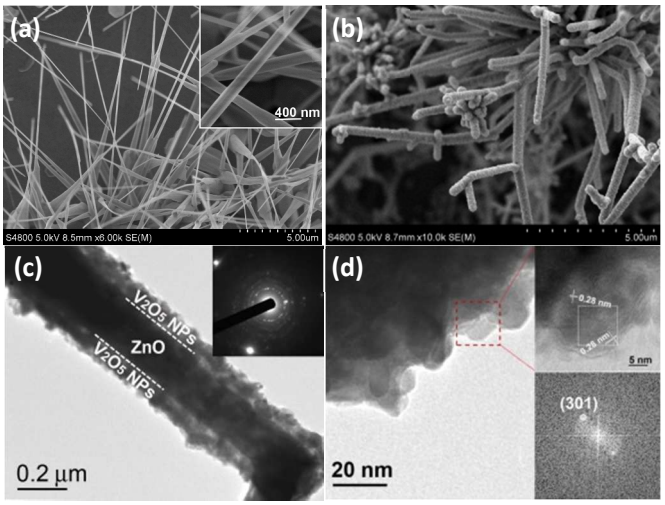

Fig. 2. (a) The SEM image of bare ZnO NRs obtained by a thermal evaporation method. SEM (b), and TEM (c) images of V_2O_5/ZnO heteronanorods oxidized at 350 °C. (d) Enlarged TEM image of the coated V_2O_5 NPs. Upper inset: High-resolution TEM image of a single V_2O_5 NPs. Lower inset: the fast Fourier transform (FFT) patterns corresponding to the white square region of the upper inset.

oxidization temperature, the oxidization treatments were performed at temperatures of 350, 420, 500 and 550 °C, respectively. The purity and crystallinity of as-prepared products were analyzed by an X-ray diffractogram. XRD pattern for bare ZnO NRs in Fig. 1a (curve A) shows only peaks indexed to wurtzite ZnO (JCPDS 36-1451) with lattice constants of a = 11.516 Å, b = 3.566 Å, c = 4.373 Å. No peaks of any other phases or impurities were detected in the spectra, revealing the high phase purity of ZnO NRs. For V_2O_5/ZnO heteronanorods obtained at 350 °C, the XRD pattern (curve B, Fig. 1a) verified there was a new phase in addition to wurtzite ZnO, which could be indexed to orthorhombic V_2O_5 (JCPDS 41-1426). When the oxidization temperature was adjusted to 420 °C and 500 °C, no characteristic peak of other phases or impurities was detected except XRD peaks indexed to V_2O_5 and ZnO, confirming the components of the V_2O_5 and ZnO in binary V_2O_5/ZnO heteronanorods. Furthermore, the diffraction intensity for V_2O_5 peaks increased gradually with the oxidization temperature, meanwhile, the corresponding FWHM (full width at half maximum) narrowed gradually (Fig. 1b). Generally, the increasing of peak intensity and the narrowing of FWHM can be attributed to the crystallinity improvement and the grain size enlargement, thus the crystallinity and size of the coated V_2O_5 NPs can be tuned by adjusting the oxidization temperature. When the oxidization temperature was increased to 550 °C, the XRD pattern of the product showed some extra sharp peaks related to $Zn_2V_2O_7$ and ZnV_2O_6 (curve E, Fig. 1a). Thus, the phase changes in products are quite sensitive to the oxidization temperature. To obtain pure V_2O_5/ZnO heteronanorods, the oxidization temperature should be controlled in an appropriate range during the oxidization process.

Fig. 2a shows a typical SEM image of bare ZnO NRs synthesized by a thermal evaporation method. It can be seen that the product is composed of a large quantity of 1D rod-like ZnO nanostructures with good quality and smooth surface. The lengths of them are from 2 to 10 μm, and their diameters range from 100 to 200 nm (see the inset of Fig. 2a). After a coating process followed by an oxidization treatment at 350 °C, V_2O_5 NPs were coated on the ZnO surface, forming V_2O_5/ZnO heteronanorods. As shown in Fig. 2b, these V_2O_5/ZnO heteronanorods still retain the initial 1D structure of ZnO NRs. However, rough surface of them can be clearly seen (Fig.2b), and their diameters also increased remarkably from ~100-200 nm to ~400 nm, confirming V_2O_5 NPs being coated on ZnO NRs. Fig. 2c shows a low-magnification TEM image of a single V_2O_5/ZnO heteronanorod, where the ZnO core has a diameter of ~200 nm and the thickness of V_2O_5 shell is ~80-120 nm. In the corresponding selected area electron-diffraction (SAED) shown in the inset of Fig. 2c, two sets of diffraction patterns are observed, the bright and clear diffraction spots belong to the single crystal ZnO NR, and the regular polycrystalline rings can be attribute to the loaded V_2O_5 NPs. The enlarged TEM image for the shell (Fig. 2d) indicates that the polycrystalline V_2O_5 shell is composed of V_2O_5 NPs with size less than 20 nm. The corresponding HRTEM image (upper inset, Fig. 2d) for the region marked in red square shows a nanoparticle with regular spacing of 0.28 nm, which is accordance with the interplanar distance of (301) plane of V_2O_5. The well-resolved fringes and the corresponding FFT patterns (lower inset of Fig. 2d) confirm the single crystallinity of the V_2O_5 particles.

As the oxidization temperature increased to 420 °C and 500 °C, respectively, other two V_2O_5/ZnO samples were obtained. As shown in Fig. 3a and 3b, morphologies of the two samples are found to be quite different from the sample of 350 °C. Although both of them have similar 1D rod-like nanostructures as the sample of 350 °C, it is found that the surface roughness of them increases remarkably. Due to the Ostwald ripening process, the coated V_2O_5 NPs grew larger with the risen oxidization temperature (Fig. 3c and 3d), leading to the increasing surface roughness. As shown in Fig. 3e and 3f, the particle size of coated V_2O_5 NPs at 350 °C is less than 20

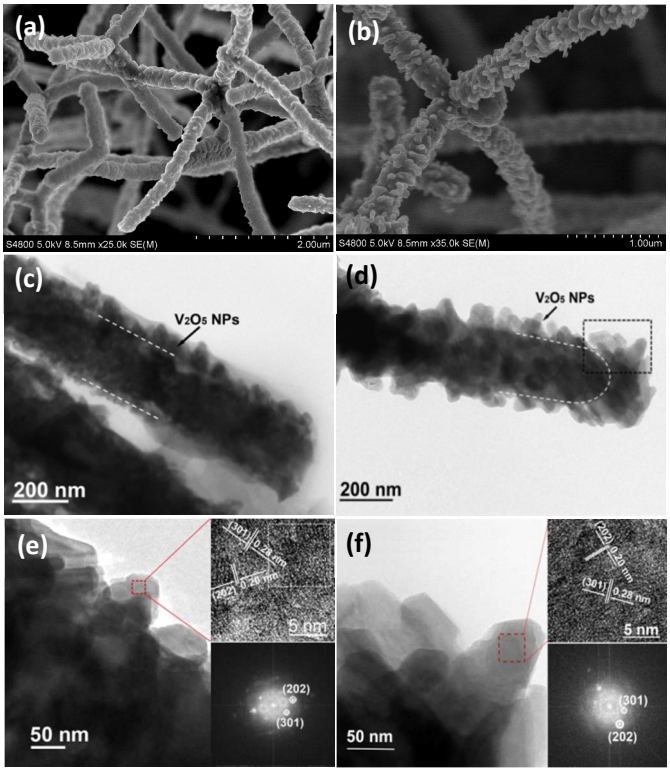

Fig. 3. SEM images for V_2O_5/ZnO heteronanorods of (a) 420 °C and (b) 500 °C. TEM images for V_2O_5/ZnO heteronanorods of (c) 420 °C and (d) 500 °C. Enlarged TEM images for coated V_2O_5 NPs in V_2O_5/ZnO heteronanorods of (e) 420 °C and (f) 500 °C. Upper insets in (e) and (f): the high-resolution TEM images for V_2O_5 NPs marked by red squares. Lower insets in (e) and (f): the corresponding FFT patterns for the white square regions in the upper insets.

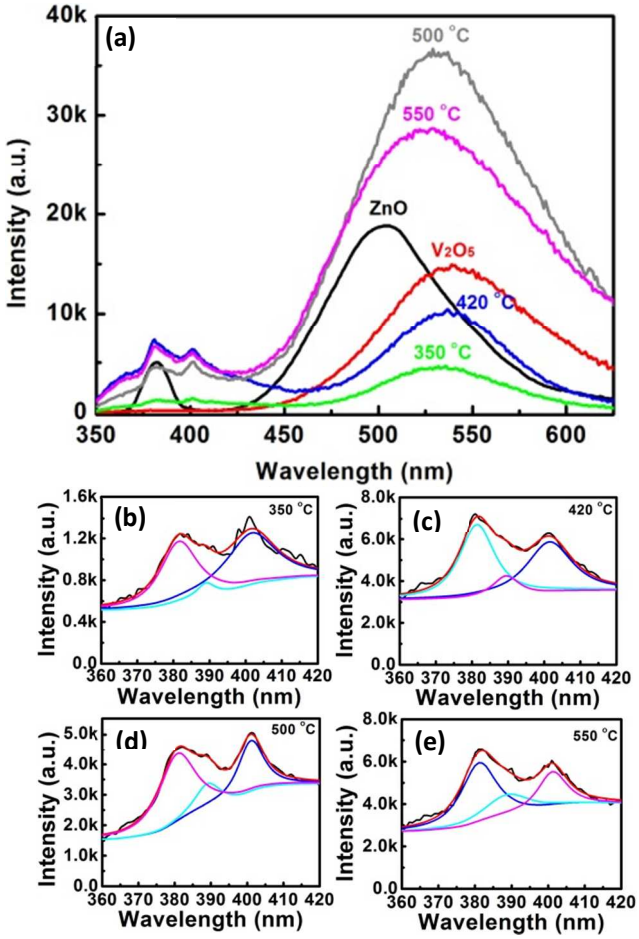

Fig. 4. (a) Room-temperature PL spectra for different V_2O_5/ZnO heteronanorods obtained at temperatures of 350, 420, 500 and 550 °C, respectively. For comparison, the PL spectra of the pure V_2O_5 and bare ZnO NRs were also figured. (b-e) Fitting ultraviolet PL spectra (360-420 nm) for different V_2O_5/ZnO heteronanorods obtained at temperatures of 350, 420, 500 and 550 °C, respectively.

nm (Fig. 2d); however, the value increased to ~40-70 nm (Fig. 3e) and then grew larger than 100 nm (Fig. 3f) when the temperature increased to 420 °C and then to 500 °C. The HRTEM images for the coated V_2O_5 NPs are shown in upper insets of Fig. 3e and 3f, corresponding to the sample of 420 °C and 500 °C, respectively. In them, the lattice fringes are observed much clearer than that in Fig. 2d, illustrating the crystallinity improvement of coated V_2O_5 NPs, in good agreement with the XRD results (Fig. 1a and 1b). Clear lattice fringes in HRTEM images (upper insets, Fig. 3e and 3f) and their corresponding FFT pattern (lower insets, Fig. 3e and 3f) reveal the single crystal of the V_2O_5 NPs, and the lattice spacing of 0.28 nm and 0.20 nm corresponds to *d* spacing of (301) and (202) planes, respectively.

PL spectra for different V_2O_5/ZnO heteronanorods of 350, 420, 500 and 550 °C are shown in Fig. 4a. For comparison, pure V_2O_5 NPs and bare ZnO NRs are also employed and their PL spectra are figured in Fig. 4a. Here, pure V_2O_5 NPs were successfully synthesized by depositing the intermediate on a silicon substrate and oxidizing them at 500 °C. As shown in Fig. 4a, pure V_2O_5 sample shows a broad visible light emission centered at 543 nm, consistent with the reported bandgap of crystal V_2O_5 of 2.3 eV. Bare ZnO NRs exhibit a narrow UV light emission with a peak at 381 nm and a broad green emission with a peak at 510 nm. The UV emission band was due to the near-band-edge (NBE) transition, and the green emission originated from defect emissions in the ZnO crystals. After coating V_2O_5 NPs on ZnO NRs, quite different PL spectra were observed as shown in Fig. 4a, and their PL spectra are noted being strongly influenced by the oxidization temperature. Compared to bare ZnO NRs, the green emission peaks for all V_2O_5/ZnO samples exhibit a significant redshift as shown in Fig. 4a. The peak redshift should be caused by the visible emission of V_2O_5 due to its relative narrow bandgap (2.3 eV). In addition, another conspicuous difference of new peak appearance was observed in the region from 350 nm to 420 nm. Unlike only one UV emission peak of bare ZnO NRs, PL spectra for all V_2O_5/ZnO samples show several emission peaks in the near UV region (Fig. 4a). The Gaussian multiple fitted curves for these peaks are figured in Fig. 4b-e, showing three emission peaks located at 381, 389 and 401 nm, respectively. The emission peak at 381 nm is attributed to the NBE emission of ZnO; however, the neighbor peaks at 389 and 401 nm cannot be attributed to ZnO, and does not appear in the PL signals of the pure V_2O_5 tested before. In previous studies about V-doped

ZnO films, PL emission peaks at 3.217 eV (~389 nm) and 3.13 eV (~401 nm) have been reported.[38, 39] In our V_2O_5/ZnO heteronanorods, some V atoms at the interface may diffuse into the ZnO core through a high-temperature oxidization process, and a thin V-doped ZnO layer should be formed at the interface of V_2O_5/ZnO. Thus, the appearance of new extra PL peaks should be closely correlated to the dopant of vanadium. The emission peak at 389 nm is attributed to the radiative recombination of the donor-acceptor pair, according to the interpretation of Singh et al..[38] The emission peak at 401 nm is attributed to the deep level emission introduced by the V impurity.

In addition, the PL intensity of V_2O_5/ZnO heteronanorods is noted to be strongly influenced by the oxidization temperature. V_2O_5/ZnO heteronanorods obtained at 350 °C showed a weakened PL emission intensity compared to bare ZnO NRs. Considering the coated V_2O_5 NPs, the weakened PL spectra should be closely related to these V_2O_5 NPs. In V_2O_5/ZnO heteronanorods of 350 °C, the size of coated V_2O_5 NPs is smaller than 20 nm, their crystallinity is the lowest (Fig. 1 and Fig. 2d), and thus the defect concentration in V_2O_5 NPs should be the highest. Furthermore, the staggered band offset at V_2O_5/ZnO interface can promote the separation of photogenerated carrier pairs. As irradiated by a laser, a part of photogenerated carries is separated at the interface, leading to a decreased recombination rate. Although other carrier pairs will recombine to excite photons from the ZnO core, these excited photons will be captured immediately by defects of V_2O_5 NPs. Therefore, a weakened PL intensity was observed and attributed to the interface carrier separation and the defect-related photon absorption. When raising the oxidization temperature to 420 °C, the PL emission intensity is observed enhanced to some extent. The raised temperature will promote V_2O_5 NPs growing larger (Fig. 3e), improve their crystalline quality, and lower the defect concentration; thus, the PL emission intensity was observed enhanced. When the oxidization temperature was further increased to 500 °C, the obtained V_2O_5/ZnO heteronanorods showed a tremendous enhancement of visible light emission, exhibiting an ~8.1 times and 3.5 times emission intensity compared with the sample of 420 °C and 500 °C, respectively; whereas, the PL peak intensity in near UV region was noted to be weakened compared to the sample of 420 °C. It is understandable that the enhancement of green light emission is partially due to the improved crystallinity of V_2O_5 NPs, while the weakened UV emission cannot be interpreted by this. Here, the ZnO core may play another important role in the enhanced green emission and the depressed near-UV emission. Actually, in the PL testing process, the external laser source excites the V_2O_5 NPs and ZnO NRs simultaneously. Then, the ZnO core and the V-doped ZnO layer at interface will emit UV light around 381, 389 and 401 nm, and V_2O_5 NPs will mainly emit visible light (2.3 eV of bandgap). Because the ZnO NRs were coated by V_2O_5 NPs, the emitted UV light will be absorbed by V_2O_5 NPs and excite V_2O_5 NPs nearly at the same time. Thus, two exciting channels for V_2O_5 NPs are formed, one is the external laser source, and

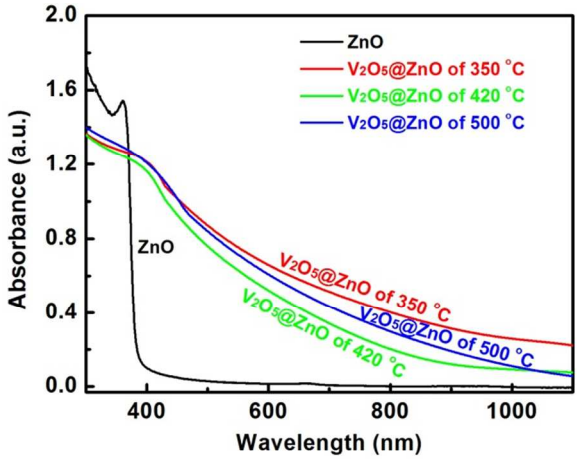

Fig. 5. UV–vis absorption spectra of bare ZnO NRs and V_2O_5/ZnO heteronanorods of 350, 420 and 500 °C, respectively.

the other is the UV light from the ZnO core and V-doped ZnO layer. Due to the resonant excitation, the PL spectrum for V_2O_5/ZnO heteronanorods of 500 °C shows a tremendous enhancement of visible light emission, meanwhile, the UV emission peaks were suppressed due to the absorption. For V_2O_5/ZnO heteronanorods obtained at 550 °C, both the UV emission and the visible emission are observed weakened to some extent, which can be attributed to the impurity appearance of $Zn_2V_2O_7$ and ZnV_2O_6.

To evaluate the photocatalytic activities, V_2O_5/ZnO heteronanorods of 350, 420 and 500 °C are selected, and their UV−vis absorption spectra are firstly measured and shown in Fig. 5. For comparison, bare ZnO NRs are also employed, but V_2O_5/ZnO heteronanorods of 550 °C are eliminated because of impurities of $Zn_2V_2O_7$ and ZnV_2O_6 existing in them. As shown in Fig. 5, bare ZnO NRs shows a sharp NBE absorption edge at ~380 nm due to the bandgap of 3.3 eV. After coating V_2O_5 NPs on ZnO NRs, the absorption edge becomes ambiguous compared to that of bare ZnO NRs. The average absorption for UV light weakens slightly, whereas the absorption in the visible range strengthens greatly, indicating their potential for the photocatalytic application with visible light. Bare ZnO NRs, pure V_2O_5 NPs, and three different V_2O_5/ZnO heteronanorods (350, 420 and 500 °C) are used as photocatalysts and compared each other. Their photocatalytic activities are evaluated in the photodegradation of MB dye in water under UV−vis light irradiation. The characteristic absorption of MB at 664 nm was used to monitor the photocatalytic degradation process. The dependencies of the degradation efficiency on irradiation time for the samples are presented in Fig. 6a. The degradation efficiency is defined as C/C_0, where C is the remaining concentration of the MB solution, and C_0 refers to the MB concentration after the equilibrium establishment between adsorption and desorption by stirring in the dark for 30 min. After adding either ZnO NRs or V_2O_5 NPs into the MB solution and keeping the solution in the dark for 30 min, a small decrease in concentration was observed due to the adsorption of MB molecules onto the photocatalyst surface. When binary

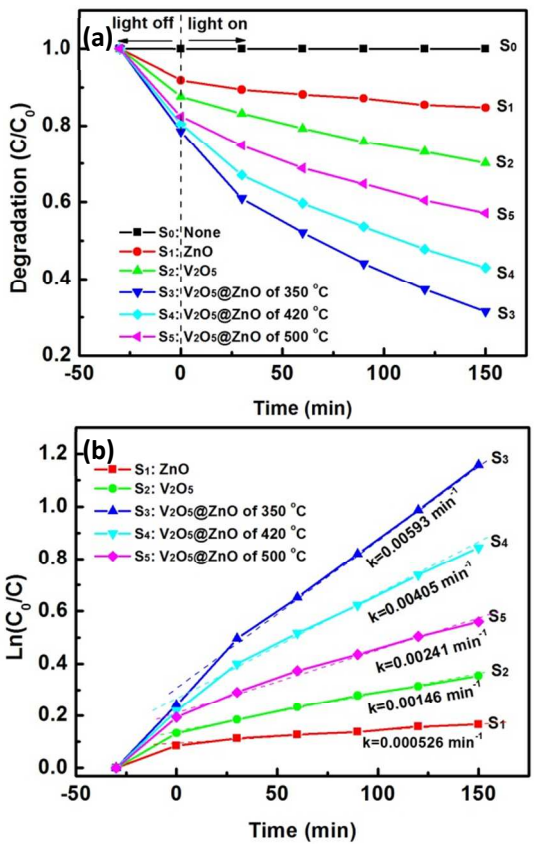

Fig. 6. (a) The decrease (C/C_0) and (b) logarithm ($\mathrm{Ln}(C_0/C)$) of the normalized concentrations vs. irradiation time for the MB solution containing different photocatalysts: S_1, bare ZnO NRs; S_2, pure V_2O_5 NPs; S_3, V_2O_5/ZnO heteronanorods of 350 °C; S_4, V_2O_5/ZnO heteronanorods of 420 °C; S_5, V_2O_5/ZnO heteronanorods of °C. The dashed lines in (b) are the linear fitting results corresponding to different photocatalysts, respectively.

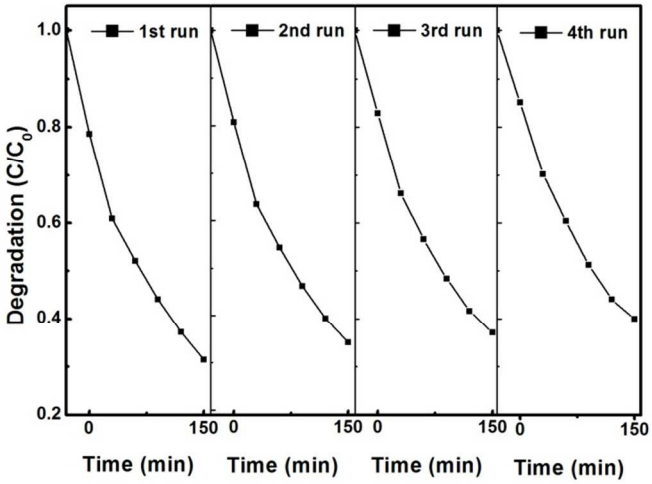

Fig. 7. Cycling runs in the photodegradation of MB in the presence of the V_2O_5/ZnO sample of 350 °C under UV-vis light irradiation.

V_2O_5/ZnO heteronanorods were added into MB solution, dramatic decreases in the MB concentration were observed, showing enhanced adsorption abilities which are beneficial in improving photocatalytic performance. In three different V_2O_5/ZnO heteronanorods, the sample of 350 °C exhibits the highest adsorption ability as shown in Fig. 6a (S_5). Because of the minimum V_2O_5 particle size and the lowest crystallinity, large defects exist on the surface of V_2O_5 NPs and act as adsorption sites, leading to the highest adsorption ability. Under the UV-vis light irradiation for 150 min, all V_2O_5/ZnO samples showed improved photocatalytic activities in comparison with either ZnO NRs or V_2O_5 NPs, illustrating a feasible way that constructing binary V_2O_5/ZnO heteronanorods to enhance the photocatalytic activity. Furthermore, it is noted that the oxidization temperature in the synthesis process also play an important role in the finial photocatalytic activity. As shown in Fig. 6a, the photocatalytic activity for different V_2O_5/ZnO heteronanorods decreases gradually with the risen oxidization temperature. V_2O_5/ZnO heteronanorods of 350 °C show the strongest photocatalytic activity and the photocatalytic activity for the sample of 500 °C is the lowest. After photocatalytic reaction for 150 min, the degradation efficiencies of three V_2O_5/ZnO samples were calculated to be ~60%, ~46.5%, and ~30.6%, corresponding to 350, 420 and 500 °C, respectively. The degradation efficiencies for ZnO NRs and V_2O_5 NPs were also calculated to be ~8.3% and ~19.8%, respectively. Fig. 5b shows the logarithm of the normalized concentrations ($\mathrm{Ln}(C_0/C)$) as a function of irradiation time for the MB solution in the presence of photocatalysts. The linear fitting indicates that MB photodegradation followed pseudo-first-order kinetics. According to the Langmuir–Hinshelwood model, the linear relationship can be described as $\mathrm{Ln}(C_0/C)=kt + A$, where k is the apparent rate constant of the degradation, C_0 and C are the concentrations of MB at initial and at a certain irradiation time t, respectively. Thus, the constant photodegradation rates, k, are calculated and included in Fig. 6b. The photodegradation rate for bare ZnO NRs and pure V_2O_5 NPs was calculated to be 0.000526 and 0.00146 min^{-1}, respectively. Clearly, the loss of MB over V_2O_5/ZnO heteronanorods was faster than their individual single-component counterparts. In a series of V_2O_5/ZnO samples, the sample of 350 °C showed the highest photodegradation rate of 0.00593 min^{-1}, and the rate decreased to 0.00405 and 0.00241 min^{-1}, when the oxidization temperature was increased to 420 °C and 500 °C, respectively. In addition, the MB solution without photocatalyst didn't show any appreciable degradation after 150 min of irradiation (curve S_0, black line in Fig. 6a). Therefore, it is concluded that the enhanced photodegradation activity indeed originates from the heteronanostructure formation and strongly depends on the microstructure of V_2O_5 NPs.

For a photocatalyst to be useful, it should be stable under repeated application. To evaluate the stability and reusability of V_2O_5/ZnO heteronanorods, the sample of 350 °C was chosen and additional experiments cycled for four times were carried out to degrade MB dye under UV−vis light irradiation. As shown in Fig. 7, V_2O_5/ZnO heteronanorods obtained at 350 °C showed a slight decline after four cycles of experimental tests: ~53.0% of the original MB was degraded after the fourth run, whereas the extent of degradation was 60.0% for the first run, confirming the stability of our V_2O_5/ZnO heteronanorods during the photocatalytic process.

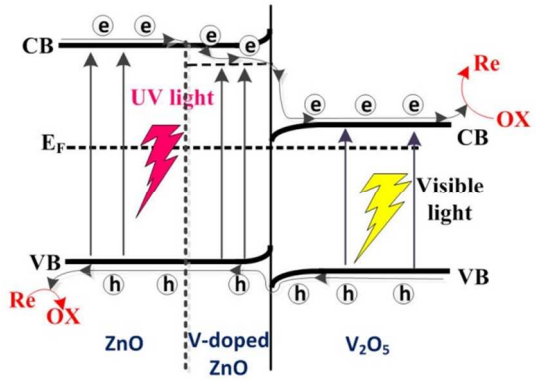

Fig. 8. Schematic diagram of the band configuration and charge-carrier transfer processes in V_2O_5/ZnO heteronanorods.

The photocatalysis result demonstrated very poor photodegradation ability for bare ZnO NRs and pure V_2O_5 NPs. However, V_2O_5/ZnO heteronanorods displayed a clear improvement of the photodegradation ability. Furthermore, it is noted that the oxidization temperature also plays an important role in the final photodegradation ability. For binary V_2O_5/ZnO samples, the improved photocatalytic activity and the temperature influence can be understood as described below. Only UV light can excite electron−hole pairs from bare ZnO NRs, and the recombination rate for either ZnO NRs or V_2O_5 NPs is too high, so the photodegradation efficiency of single-component photocatalysts is very poor. For V_2O_5/ZnO heteronanorods, the schematic diagram for the band configuration is shown in Fig. 8, where a V-doped ZnO layer is formed near the interface as revealed in the PL spectra (Fig. 4). It is well known that the Fermi level for two different components will equilibrate when they encounter each other. Clearly, different components of ZnO, V-doped ZnO, and V_2O_5 have essentially the same Fermi energy level at the interface, the doped V atoms provide some deep levels near the interface, and a staggered band offset is formed there. The equilibrium alignment of the Fermi level creates a built-in electric field in the space charge region near the ZnO/V_2O_5 interface. When V_2O_5/ZnO heteronanorods were irradiated with UV-vis light, electrons in V_2O_5 and ZnO are excited by visible and UV light, respectively. Because the conduction and valence bands of V_2O_5 lie below the energy band of ZnO (Fig. 8), photogenerated electrons with energy higher than the built-in field can easily cross the interface and transfer from ZnO to V_2O_5. Likewise, the holes excited from V_2O_5 can easily cross the interface and transfer to the valence band of ZnO. Moreover, deep levels provided by the doped V atoms can also decrease the built-in field near the interface, provide a stair for electron transfer from ZnO to V_2O_5, and ultimately, promote the separation of photogenerated carriers. Thus, elevated photocatalytic abilities are obtained in V_2O_5/ZnO heteronanorods. Moreover, the influence of the oxidization temperature can also be interpreted by changes in the size and the crystallinity of coated V_2O_5 NPs. When the oxidization temperature was set at 350 °C, the coated V_2O_5 NPs showed a particle size smaller than 20 nm, and their crystallinity is relatively low. The small particle size less than 20 nm not only increased the contact area between V_2O_5 NPs and the MB solution, but also shortens the transfer distance for photogenerated electrons emigrating from the inner to the surface. In the photochemical reaction, the photogenerated carrier pairs are separated at V_2O_5/ZnO interface. These separated electrons are injected into V_2O_5 NPs, emigrate to the particle surface, and ultimately, react with MB molecules. The relative low crystallinity of V_2O_5 NPs leads to a high defect concentration. As shown in the TEM image of Fig. 2d, the coated V_2O_5 NPs are single crystallinity; thus, the defects should be mainly on the surface not in the bulk. These surface defects acts as reaction sites, where the moving electrons can be easily captured and react with adsorbed MB molecules, so the photochemical reaction is accelerated and the elevated photocatalytic activity was obtained. When the oxidization temperature increased to 420 °C and then to 500 °C, V_2O_5 NPs grew bigger and bigger, meanwhile, the crystallinity was improved gradually. Thus, the defect concentration is lowered, and the emigration distance for photogenerated electrons moving to the surface is prolonged, resulting in the gradually decreased photocatalytic activity.

Conclusions

In summary, V_2O_5/ZnO heteronanorods were prepared via a coating process followed by a thermal oxidization. XRD, SEM and TEM analyses revealed that the interior ZnO cores were coated by a large quantity of V_2O_5 NPs. When the oxidization temperature was increased from 350 °C to 420 °C and then to 500 °C, three different V_2O_5/ZnO heteronanorods were obtained. In them, coated V_2O_5 NPs were observed growing with the oxidization temperature; meanwhile, their crystallinity was improved gradually. PL and photocatalysis investigation indicates that coating V_2O_5 NPs on ZnO NRs can remarkably change the PL signals and the photocatalytic activity. New extra PL emission peaks located at 389 and 401 nm were observed, the PL intensity strongly depended on the oxidization temperature, and the sample of 500 °C exhibited a tremendously enhanced visible emission. In addition, these binary V_2O_5/ZnO samples showed remarkably enhanced photocatalytic activities compared to bare ZnO NRs and pure V_2O_5 NPs. Moreover, their photocatalytic activities are found strongly depending on the oxidization temperature, the sample of 350 °C showed the highest photocatalytic activity, and activities for the other two samples decreased gradually with the oxidization temperature. The appearance of extra PL peaks, the variation in PL intensity, and different photocatalytic activities can be interpreted by the V-doped ZnO layer formed at interface, the decreased defect concentration in V_2O_5 NPs, and the improvement of the particle crystallinity.

Acknowledgements

The authors acknowledge financial support from the NSF of China (Grant Nos. 61204018, 61274014, and 61474043), the NSF of Jiangsu Province (Grant No. BK20141239), Innovation Research Project of Shanghai Education Commission (Grant No. 13zz033), Education Committee of Jiangsu Province (Grant No. 14KJB510029), Project of Key Laboratory of Polar Materials and Devices (Grant No. KFKT2014003), Doctoral Scientific Research Funds of Nantong University (13B23 and 13B25), and Undergraduate Training Programs for Innovation and Entrepreneurship of Jiangsu Province (201410304019Z).

Notes and references

[a] *School of Electronics and Information, Nantong University, Nantong, 226019, P. R. China.*

[b] *Key Laboratory of Polar Materials and Devices (Ministry of Education of China), Department of Electronic Engineering, East China Normal University, Shanghai, 200241, P. R. China. Fax: +86-21-54345198; Tel: 13611980114; E-mail: yk5188@263.net*

1. Y. B. Guo, H. B. Liu, Y. J. Li, G. X. Li, Y. J. Zhao, Y. L. Song and Y. L. Li, *J. Phys. Chem. C*, 2009, **113**, 12669-12673.
2. Z. Li, Z. Hu, J. Peng, C. Wu, Y. Yang, F. Feng, P. Gao, J. Yang and Y. Xie, *Adv. Funct. Mater.*, 2014, **24**, 1821-1830.
3. L. Ming, Y. Junyou, Q. Qiuliang, Z. Pinwen and L. Weixin, *J. Power Sources*, 2015, **273**, 848-856.
4. Z. B. Yu, Y. P. Xie, G. Liu, G. Q. Lu, X. L. Ma and H.-M. Cheng, *J. Mater. Chem. A*, 2013, **1**, 2773-2776.
5. L. Lou, K. Yu, Z. Zhang, B. Li, J. Zhu, Y. Wang, R. Huang and Z. Zhu, *Nanoscale*, 2011, **3**, 2315-2323.
6. H. Long, G. J. Fang, S. Z. Li, X. M. Mo, H. N. Wang, H. H. Huang, Q. K. Jiang, J. B. Wang and X. Z. Zhao, *IEEE. Electr. Device. Lett.*, 2011, **32**, 54-56.
7. Z. Dong, X. Lai, J. E. Halpert, N. Yang, L. Yi, J. Zhai, D. Wang, Z. Tang and L. Jiang, *Adv. Mater.*, 2012, **24**, 1046-1049.
8. Z. L. Wang and J. H. Song, *Science*, 2006, **312**, 242-246.
9. V. Quang Dang, D.-I. Kim, L. Thai Duy, B.-Y. Kim, B.-U. Hwang, M. Jang, K.-S. Shin, S.-W. Kim and N.-E. Lee, *Nanoscale*, 2014, **6**, 15144-15150.
10. A. Gurlo, *Nanoscale*, 2011, **3**, 154-165.
11. S. Ma, J. Xue, Y. Zhou and Z. Zhang, *J. Mater. Chem. A*, 2014, **2**, 7272-7280.
12. X. Guo, H. Zhu and Q. Li, *Applied Catalysis B: Environmental*, 2014, **160-161**, 408-414.
13. K. Qu, C. Li, K. Hou, X. Yang, J. Zhang, W. Lei, X. Zhang, B. Wang and X. W. Sun, *Appl. Phys. Lett.*, 2008, **93**, 253501.
14. N. Y. Garces, L. Wang, L. Bai, N. C. Giles, L. E. Halliburton and G. Cantwell, *Appl. Phys. Lett.*, 2002, **81**, 622.
15. X. Y. Chen, F. Fang, A. M. C. Ng, A. B. Djurišić, W. K. Chan, H. F. Lui, P. W. K. Fong, C. Surya and K. W. Cheah, *Thin Solid Films*, 2011, **520**, 1125-1130.
16. D. Qiu, P. Yu, Y. Jiang and H. Wu, *J. Mater. Sci. Technol.*, 2006, **22**, 541-545.
17. K. Sowri Babu, A. Ramachandra Reddy, C. Sujatha, K. V. G. Reddy and A. N. Mallika, *Mater. Lett.*, 2013, **110**, 10-12.
18. K. Pita, P. Baudin, V. Quang Vinh, R. Aad, C. Couteau and G. Lerondel, *Nanoscale Res. Lett.*, 2013, **8**, 517.
19. A. Dev, R. Niepelt, J. P. Richters, C. Ronning and T. Voss, *Nanotechnology*, 2010, **21**, 065709.
20. A. Dev, J. P. Richters, J. Sartor, H. Kalt, J. Gutowski and T. Voss, *Appl. Phys. Lett.*, 2011, **98**, 131111.
21. M. Mahanti, T. Ghosh and D. Basak, *Nanoscale*, 2011, **3**, 4427-4433.
22. Y. Jinkyoung, C. Bonghwan, T. Wei, J. Taiha, D. Le Si and Y. Gyu-Chul, *Appl. Phys. Lett.*, 2012, **100**, 223103.
23. C. Jin, H. Kim, H.-Y. Ryu, H. W. Kim and C. Lee, *J. Phys. Chem. C*, 2011, **115**, 8513-8518.
24. Q. Kuang, Z. Y. Jiang, Z. X. Xie, S. C. Lin, Z. W. Lin, S. Y. Xie, R. B. Huang and L. S. Zheng, *J. Am. Chem. Soc.*, 2005, **127**, 11777-11784.
25. V. G. Pol, S. V. Pol, J. M. Calderon-Moreno and A. Gedanken, *J. Phys. Chem. C*, 2009, **113**, 10500-10504.
26. Y. Hu, Z. Li, Z. Zhang and D. Meng, *Appl. Phys. Lett.*, 2009, **94**, 103107.
27. A. Othonos, C. Christofides and M. Zervos, *Appl. Phys. Lett.*, 2013, **103**, 133112.
28. C. W. Zou, X. D. Yan, J. M. Bian and W. Gao, *Opt. Lett.*, 2010, **35**, 1145-1147.
29. H. Kim, C. Jin, S. Park, W. I. Lee and C. Lee, *J. Nanosci. Nanotechnol.*, 2014, **14**, 5181-5186.
30. A. B. Djurisic, X. Chen, Y. H. Leung and A. Man Ching Ng, *J. Mater. Chem.*, 2012, **22**, 6526-6535.
31. S. Liu, C. Li, J. Yu and Q. Xiang, *CrystEngComm*, 2011, **13**, 2533-2541.
32. M. Mapa and C. S. Gopinath, *Chem. Mater.*, 2008, **21**, 351-359.
33. Z. W. Deng, M. Chen, G. X. Gu and L. M. Wu, *J. Phys. Chem. B*, 2008, **112**, 16-22.
34. L. N. Wang, Y. Y. Zheng, X. Y. Li, W. J. Dong, W. H. Tang, B. Y. Chen, C. R. Li, X. Li, T. R. Zhang and W. Xu, *Thin Solid Films*, 2011, **519**, 5673-5678.
35. Y.-C. Huang, S.-Y. Chang, C.-F. Lin and W. J. Tseng, *J. Mater. Chem.*, 2011, **21**, 14056-14061.
36. S. Jung and K. Yong, *Chem. Commun.*, 2011, **47**, 2643-2645.
37. C. W. Zou, Y. F. Rao, A. Alyamani, W. Chu, M. J. Chen, D. A. Patterson, E. A. C. Emanuelsson and W. Gao, *Langmuir*, 2010, **26**, 11615-11620.
38. S. Shubra, N. Daisuke, S. Kentaro, O. Tatsuo and M. S. R. Rao, *New J. Phys.*, 2010, **12**, 023007.
39. G. Jayalakshmi, K. Saravanan, S. Balakumar and T. Balasubramanian, *Vacuum*, 2013, **95**, 66-70.

